Charmed hypernuclei within density-dependent relativistic mean-field theory

Wei Yang (杨威), Shi Yuan Ding (丁士缘), and Bao Yuan Sun (孙保元)*
MOE Frontiers Science Center for Rare Isotopes, Lanzhou University, Lanzhou 730000, China
and School of Nuclear Science and Technology, Lanzhou University, Lanzhou 730000, China

(Received 27 June 2024; revised 16 September 2024; accepted 1 November 2024; published 20 November 2024)

The charmed Λ_c^+ hypernuclei were investigated within the framework of the density-dependent relativistic mean-field (DDRMF) theory. Starting from the empirical hyperon potential in symmetric nuclear matter, obtained through microscopic first-principle calculations, two sets of $\Lambda_c N$ effective interactions were derived by fitting the potentials at a certain density either with minimal model uncertainty (Fermi momentum $k_{F,n} = 1.05\ \mathrm{fm}^{-1}$) or nearby the saturation point ($k_{F,n} = 1.35\ \mathrm{fm}^{-1}$). These DDRMF models were then used to explore the $\Lambda_c N$ effective interaction uncertainties on the description of hypernuclear bulk and single-particle properties. A systematic investigation was conducted on the existence of bound Λ_c^+ hypernuclei. The dominant factors affecting the existence and stability of hypernuclei were analyzed from the perspective of the Λ_c^+ potential. It was found that the hyperon potential is influenced not only by the Coulomb repulsion, but by an extra contribution from the rearrangement terms due to the density dependence of the meson-baryon coupling strengths. Therefore, the rearrangement term significantly impacts the stability description for light hypernuclei, while for heavier hypernuclei the contribution from Coulomb repulsion becomes increasingly significant and eventually dominant. The discussion then focuses on the bulk and single-particle properties of charmed hypernuclei using these models. It is shown that different treatments of nuclear medium effects could lead to discrepancies in the theoretical description of hypernuclear structures, even when different models yield similar hyperon potentials within nuclear matter, indicating that constraints on the $\Lambda_c N$ interaction at finite densities are crucial for the study of Λ_c^+ hypernuclear structures.

DOI: 10.1103/PhysRevC.110.054320

I. INTRODUCTION

Since the discovery of hyperons in the early 1950s, particles containing strange quarks have attracted significant attention from both experimental and theoretical physicists [1]. Hyperons, which carry new degrees of freedom beyond nucleons, are free from the nucleon's Pauli exclusion principle. This property enables the hyperon within hypernuclei to penetrate deep into the interior of atomic nuclei, acting as sensitive probes for studying the nuclear structure and specific nuclear features. Research on hyperons within nuclei helps us understand the baryon-baryon interactions in nuclear matter and their impact on nuclear properties [2,3]. This knowledge is also crucial for understanding the matter in neutron stars, where hyperons may appear [4–6]. So far, experimental data on hypernuclei with strangeness $S = -1$ (Λ and Σ hypernuclei) and $S = -2$ ($\Lambda\Lambda$ and Ξ hypernuclei) have been obtained [7–14]. Based on these experimental data, various theoretical frameworks have been employed to study the hypernuclear structures and neutron star matter containing hyperons, such as the shell model [15–17], the Skyrme-Hartree-Fock model [18–20], the relativistic mean-field (RMF) theory [20–26], the quark mean-field model (QMF) [27], as well as the relativistic Hartree-Fock (RHF) theory [28].

In addition to the above-mentioned hyperons containing strange quarks, theory has also predicted a particle containing a charmed quark, whose composition is very similar to that of the Λ hyperon. It can be viewed as the strange quark in the Λ hyperon being replaced by a charmed quark, and was experimentally evidenced in the early 1970s [29,30]. Due to their composition, charmed particles may exhibit behaviors similar to Λ hyperons, such as moving deep into the nucleus to form charmed hypernuclei, providing us with another unique perspective for studying nuclear structure. Research on the charmed hypernuclei helps us to understand the charmed baryon-nucleon interactions within the SU(4) symmetry framework, and the extraction of relevant interactions provides opportunity to test physics such as dynamical chiral symmetry breaking (DCSB) [31,32].

Experimental detection provides a direct and effective approach to study hypernuclear structure. In the past, it was suggested that charmed hypernuclei could be produced through the charm exchange reaction, namely the (D, π) reaction [33,34]. Due to the extremely short lifetimes and high momenta of D mesons, they are difficult to capture by nucleons in these reactions, which poses significant challenges for the formation and study of charmed hypernuclei. Over the past few decades, only a few possible signals of charmed hypernuclei have been detected, at Dubna [35,36]. In recent years, another effective method for producing charmed hypernuclei, namely the antiproton-nucleus collision method, has

*Contact author: sunby@lzu.edu.cn

been proposed. This method does not require the production of additional D mesons, thereby increasing the possibility of forming charmed hypernuclei [37]. The $\bar{\text{P}}$ANDA experiment at FAIR (GSI) is expected to study the production of charmed hypernuclei using the new method [37], and the experimental feasibility was also theoretically analyzed [38]. Furthermore, the J-PARC facility, which can provide high-intensity and high-momentum proton beams, also offers an ideal experimental platform for the production of charmed hypernuclei [39,40]. With the gradual construction and upgrading of facilities for radioactive ion beams, accurate information about the charmed hypernuclei is expected to be obtained in the future, providing strong support for the study of hypernuclear structures.

Given the limited experimental data, theoretical research on charmed hypernuclei is crucial as it both deepens our understanding and provides valuable guidance for future experiments. Since the Λ_c^+ particle carries the same positive charge as the proton, its Coulomb interaction with protons in the nucleus affects the stability of Λ_c^+ hypernuclei, making it challenging to form a hypernucleus by binding with nucleons. Consequently, after the experimental observation of charmed particles, theoretical physicists have primarily focused on discussing the existence and stability of Λ_c^+ hypernuclei [29]. In 1977, the possible existence of Λ_c^+ hypernuclei was first explored theoretically based on SU(4) symmetry [41]. Subsequently, many theoretical models have been extended to include the Λ_c^+ degree of freedom, systematically investigating Λ_c^+ hypernuclei from light to heavy. For lighter hypernuclei, systematic studies have been conducted using few-body methods based on cluster models and Faddeev equations [42–45]. Recently, in-depth discussions on the existence of the ${}^{3}_{\Lambda_c}\text{H}$ hypernucleus have been conducted based on the quark-delocalization color-screening (QDCSM) model [46].

Density functional theory (DFT) is an ideal approach for studying medium and heavy hypernuclei, as it can describe the single-particle and collective properties of finite nuclei in almost the entire nuclear chart. In previous work, several density functional theory approaches have been extended to study the structure of Λ_c^+ hypernuclei, such as the quark meson coupling (QMC) model [38,47], the quark mean-field (QMF) model [48], the Skyrme-Hartree-Fock (SHF) approach [49,50], and the relativistic mean-field (RMF) approach [51,52]. In addition to DFT, the perturbation many-body approach based on the nuclear matter G-matrix has also seen further development recently, achieving a unified and self-consistent description of Λ_c^+ hypernuclear structures from light to heavy [53,54]. Based on these theoretical models, detailed analyses have been carried out on the existence and stability of charmed hypernuclei, and the impurity effects induced by the introduction of Λ_c^+ particles were further investigated.

Despite extensive theoretical analyses of the Λ_c^+ hypernuclear structure, the lack of experimental information has made it difficult to construct the $\Lambda_c N$ interaction from a unified starting point, which has also led to additional uncertainties in the results of various theoretical models for the Λ_c^+ hypernuclear structure. In early works, pivotal information on the $\Lambda_c N$ interaction, such as low-energy scattering parameters and hyperon potentials, was directly obtained based on SU(4) symmetry [41,42,55]. Some studies have attempted to construct the $\Lambda_c N$ interaction by scaling the Λ_c^+ hyperon potential to that of the Λ hyperon or using other specific values, but the significant differences in the constructed interactions have also introduced large uncertainties in the theoretical analysis of hypernuclear structure [50,52]. Recently, lattice QCD simulations have explored the $\Lambda_c N$ interaction under different unphysical pion masses. Subsequent work used chiral effective field theory to extrapolate the simulation results, obtaining the effective $\Lambda_c N$ interaction at a pion mass of $m_\pi = 138$ MeV [56]. Building upon this, the extrapolated results including the $\Sigma_c N$ channel have been studied, and it was found that the $\Sigma_c N$ coupling has little impact on the $\Lambda_c N$ interaction at low energies [54]. Additionally, the properties of Λ_c^+ hypernuclear bound states and resonance states were explored by considering different symmetries in the effective Lagrangian [57,58]. Based on the derived two-body $\Lambda_c N$ interaction, various theoretical models have been employed to obtain information on Λ_c^+ hyperon in nuclear matter. For example, analyses based on SU(4) symmetry indicate that the Λ_c^+ hyperon potential in nuclear matter ranges from -20 to -28 MeV [42,55,59,60]. Recent lattice QCD simulations and their extrapolated results suggest Λ_c^+ potential depth of less than 20 MeV [54,61,62], consistent with results obtained using parity-projected QCD sum rules, which propose an attractive potential of $U_{\Lambda_c} \approx -20$ MeV at normal nuclear density [63].

In addition to the $\Lambda_c N$ interaction, a reliable description of hypernuclear structure also relies on the adopted nuclear many-body methods. As a significant branch of density functional theory, the RMF approach is capable of describing not only infinite nuclear matter but the single-particle and collective properties of finite nuclei in almost the entire nuclear chart, and has been extended to the study of strangeness degrees of freedom [26,64–72]. The RMF approach with a nonlinear coupling extension was extended to study the structure of Λ_c^+ hypernuclei [51,52]. However, due to the lack of experimental information, the construction of the $\Lambda_c N$ interaction lacks a reasonable basis, resulting in significant uncertainties in the results. It is then expected that one should start from a more reasonable $\Lambda_c N$ interaction and combine it with theoretical models to achieve a reliable description of hypernuclear structure.

Considering that the hyperon is located within the nucleus, the $\Lambda_c N$ interaction is significantly affected by the nuclear medium, and different treatments for nuclear in-medium effects need to be carefully discussed regarding their impact on the bulk and single-particle properties of Λ_c^+ hypernuclei. Microscopic calculations based on the Dirac-Brueckner-Hartree-Fock (DBHF) theory indicate that nuclear in-medium effects have a significant impact on the description of nuclear structure [73]. By treating the meson-nucleon coupling strengths as functions of the baryon density, nuclear in-medium effects can be effectively considered. The density-dependent relativistic mean-field (DDRMF) and density-dependent relativistic Hartree-Fock (DDRHF) theories, developed based on this idea, achieve a self-consistent and unified description at different nuclear densities by introducing density-dependent meson-nucleon coupling strengths [73,74].

Numerous related studies have been conducted in dense matter and finite nuclei with DDRMF methods. For instance, they have explored nuclear symmetry energy [75–81], nucleon effective mass [74,82], liquid-gas phase transition [83–85], equation of state (EOS) of dense matter [79,86,87], neutron stars [81,88–90], shell evolution [91–93], neutron skin effects [89,94], and novel features in exotic nuclei [95–97]. Besides, density-dependent couplings fundamentally alter the balance between attraction and repulsion in nuclear forces, thereby affecting the description of finite nuclear structure and nuclear matter properties at different density circumstances. For example, a new type of density-dependent effective interaction DD-LZ1 was proposed by adopting a unique density-dependent form, which solves the common problem of $Z = 58, 92$ pseudoshell closures within the RMF framework, and plays a role in describing the crust of neutron stars and the maximum mass of hyperonic neutron stars [98,99]. As a further extension, the DDRMF/DDRHF theories were recently applied to the study of single-Λ hypernuclear structures, with a focus on the impact of in-medium effects on hyperon single-particle properties [26,28]. It is then expected that the details of effective nuclear forces in the medium impact the description of Λ_c^+ hypernuclear structures as well.

In this work, the stability and properties of Λ_c^+ hypernuclei are investigated using the DDRMF theory. The $\Lambda_c N$ effective interactions at finite densities are determined by fitting the empirical Λ_c^+ potential with a microscopic first-principles calculation in symmetric nuclear matter as provided by Ref. [54]. According to the behavior of the constraint potential, we select the reference values at Fermi momentum of either $k_{F,n} = 1.05\ \text{fm}^{-1}$ or $k_{F,n} = 1.35\ \text{fm}^{-1}$ as the fitting target. The obtained sets of DDRMF effective interactions enable us to investigate the impact of density-dependent coupling strengths on the description of charmed hypernuclei, as well as the model uncertainty due to the selection of $\Lambda_c N$ and NN effective interactions. Then the impurity effects due to the introduction of Λ_c^+ hyperon will be studied. This paper is organized as follows. In Sec. II, we introduce the framework of the DDRMF model for the charmed hypernuclei. In Sec. III, the determination of $\Lambda_c N$ interaction and the calculated properties of the charmed hypernuclei is discussed. Finally, a summary is provided in Sec. IV.

II. THEORETICAL FRAMEWORK

In this section, we briefly introduce the general formalism of the DDRMF theory incorporating the Λ_c^+ hyperon degrees of freedom, which starts from the following Lagrangian density:

$$\mathscr{L} = \mathscr{L}_B + \mathscr{L}_\varphi + \mathscr{L}_I. \tag{1}$$

The terms of the free fields are given by

$$\mathscr{L}_B = \sum_B \bar{\psi}_B(i\gamma^\mu\partial_\mu - M_B)\psi_B, \tag{2}$$

$$\begin{aligned}\mathscr{L}_\varphi = &+\frac{1}{2}\partial^\mu\sigma\partial_\mu\sigma - \frac{1}{2}m_\sigma^2\sigma^2\\ &-\frac{1}{4}\Omega^{\mu\nu}\Omega_{\mu\nu} + \frac{1}{2}m_\omega^2\omega^\mu\omega_\mu\\ &-\frac{1}{4}\vec{R}^{\mu\nu}\cdot\vec{R}_{\mu\nu} + \frac{1}{2}m_\rho^2\vec{\rho}^\mu\cdot\vec{\rho}_\mu\\ &+\frac{1}{2}\partial^\mu\vec{\delta}\partial_\mu\vec{\delta} - \frac{1}{2}m_\delta^2\vec{\delta}^2\\ &-\frac{1}{4}F^{\mu\nu}F_{\mu\nu},\end{aligned} \tag{3}$$

where index B (and later B') represents either a nucleon N or the charmed baryon Λ_c^+, and Σ_B represents the sum over nucleons (n, p) and the charmed baryon (Λ_c^+). The masses of baryons and mesons are given by M_B and m_ϕ $(\phi = \sigma, \omega^\mu, \vec{\rho}^\mu, \vec{\delta})$, respectively. Additionally, $\Omega^{\mu\nu}$, $\vec{R}^{\mu\nu}$, and $F^{\mu\nu}$ are the field tensors of the vector mesons ω^μ, $\vec{\rho}^\mu$ and the photon A^μ, respectively. The interaction between baryons and mesons (photon) can be expressed as $\mathscr{L}_I$,

$$\begin{aligned}\mathscr{L}_I = &\sum_B \bar{\psi}_B(-g_{\sigma B}\sigma - g_{\omega B}\gamma^\mu\omega_\mu - eQ_B\gamma^\mu A_\mu)\psi_B\\ &+\sum_N \bar{\psi}_N(-g_{\delta N}\vec{\tau}_N\cdot\vec{\delta} - g_{\rho N}\gamma^\mu\vec{\tau}_N\cdot\vec{\rho}_\mu)\psi_N.\end{aligned} \tag{4}$$

Here $g_{\phi B}$ $(g_{\phi N})$ represents the coupling strengths for various meson-baryon channels, and $\vec{\tau}_N$ is the isospin operator with the third component $\tau_{3,N} = 1$ for the neutron, $\tau_{3,N} = -1$ for the proton. To maintain the simplicity of the theoretical framework, we define the symbols Q_N for nucleons, $Q_N = \frac{1-\tau_{3,N}}{2}$, and Q_{Λ_c} for Λ_c^+ hyperons, $Q_{\Lambda_c} = 1$. Within the framework of the RMF theory, an additional coupling term between hyperons and the ω-tensor is often considered to ensure that the spin-orbit splitting of hyperons such as the Λ aligns with experimental results [67,68,100,101]. Due to the larger Λ_c^+ hyperon mass $M_{\Lambda_c} = 2286.5$ MeV [102], the spin-orbit splitting for the Λ_c^+ is significantly reduced compared to the Λ, making this effect negligible [48–50]. Therefore, we have disregarded the ω-tensor coupling in this work.

In the density-dependent relativistic mean-field theory, the meson-baryon (nucleon) coupling strength is treated as a function of the baryon density ρ_b. This approach phenomenologically incorporates the nuclear in-medium effects. Specifically, for the isoscalar mesons (σ and ω^μ), their coupling strengths with baryons can generally be expressed as

$$g_{\phi B}(\rho_b) = g_{\phi B}(0)a_{\phi B}\frac{1 + b_{\phi B}(\xi + d_{\phi B})^2}{1 + c_{\phi B}(\xi + e_{\phi B})^2}, \tag{5}$$

where $\xi = \rho_b/\rho_0$ with ρ_0 being the saturation density of the nuclear matter, and $g_{\phi B}(0)$ are the coupling strengths at $\rho_b = 0$. It is worth noting that, aside from the effective interaction DD-MEδ [78], the other Lagrangians used in this work have $e_{\phi B}$ equal to $d_{\phi B}$ in Eq. (5). Furthermore, for the isovector mesons ($\vec{\delta}$ and $\vec{\rho}^\mu$), the effective interaction DD-MEδ uses a form that is consistent with the isoscalar mesons, whereas the other effective interactions follow an exponential decay form, which can be expressed as

$$g_{\phi B}(\rho_b) = g_{\phi B}(0)e^{-a_{\phi B}\xi}. \tag{6}$$

Based on the Lagrangian density $\mathscr{L}$ of Eq. (1), the effective Hamiltonian operator for the Λ_c^+ hypernucleus can be derived through the general Legendre transformation. It can be written as follows

$$\begin{aligned}\hat{H} &= \int dx \sum_B \bar{\psi}_B(x)(-i\boldsymbol{\gamma}\cdot\nabla + M_B)\psi_B(x)\\ &\quad + \frac{1}{2}\int dx\,dx' \sum_{BB'}\sum_{\varphi}[\bar{\psi}_B\mathscr{G}_{\varphi B}\psi_B]_x\\ &\quad \times D_\varphi(x,x')[\bar{\psi}_{B'}\mathscr{G}_{\varphi B'}\psi_{B'}]_{x'},\end{aligned} \tag{7}$$

where x is the four-vector $(t, \boldsymbol{x})$ and $\varphi = \sigma, \omega^\mu, \vec{\rho}^\mu, \vec{\delta}, A^\mu$. The interaction vertices for various meson-baryon (photon-baryon) coupling channels are denoted as $\mathscr{G}_{\varphi B}(x)$, and D_φ are defined as the meson (photon) propagators [28]. Considering the simplicity of the theoretical framework, only the form for the Λ_c^+ will be provided, and the specifics of nucleon part are given in Refs. [26,28]. Since the Λ_c^+ is a charged particle with zero isospin, it only engages in the interactions with isoscalar mesons (σ and ω^μ) and photon. Consequently, the interaction vertices of the Λ_c^+ hyperon with various mesons (photon) are given by

$$\mathscr{G}_{\sigma\Lambda_c}(x) = +g_{\sigma\Lambda_c}(x), \tag{8a}$$

$$\mathscr{G}^\mu_{\omega\Lambda_c}(x) = +g_{\omega\Lambda_c}(x)\gamma^\mu, \tag{8b}$$

$$\mathscr{G}^\mu_{A\Lambda_c}(x) = +eQ_{\Lambda_c}\gamma^\mu. \tag{8c}$$

Under the no-sea approximation, the hyperon field operator ψ_{Λ_c} can be expanded using the positive energy solutions

$$\psi_{\Lambda_c}(x) = \sum_i f_i(\boldsymbol{x})e^{-i\epsilon_i t}c_i. \tag{9}$$

Here, $f_i(\boldsymbol{x})$ denotes the Dirac spinor, and c_i represents the annihilation operator for state i. The energy functional E of the hypernuclear system can be obtained by taking the expectation value of the Hamiltonian operator with respect to the Hartree-Fock ground state $|\Phi_0\rangle$. Under the spherical approximation, the Dirac spinor $f_i(\boldsymbol{x})$ of the Λ_c^+ hyperon is expanded in the following form:

$$f_{n\kappa m}(\boldsymbol{x}) = \frac{1}{r}\begin{pmatrix} iG_{a,\Lambda_c}(r)\Omega_{\kappa m}(\vartheta,\varphi)\\ F_{a,\Lambda_c}(r)\Omega_{-\kappa m}(\vartheta,\varphi)\end{pmatrix}. \tag{10}$$

Here, the index a comprises a set of good quantum numbers $(n\kappa) = (njl)$, with $\Omega_{\kappa m}$ is the spherical spinor. Correspondingly, the propagator in Eq. (7) can be expanded in terms of spherical Bessel (R_{LL}) and spherical harmonic (Y_{LM}) functions as

$$D_\varphi(\boldsymbol{x},\boldsymbol{x}') = \sum_{L=0}^{\infty}\sum_{M=-L}^{L}(-1)^M R^\varphi_{LL}(r,r')Y_{LM}(\boldsymbol{\Omega})Y_{L-M}(\boldsymbol{\Omega}'), \tag{11}$$

where $\boldsymbol{\Omega} = (\vartheta, \varphi)$, and R_{LL} contains the modified Bessel functions I and K [103,104].

The single-particle properties of the Λ_c^+ hyperon can be determined by solving the Dirac equation,

$$\begin{aligned}&\varepsilon_{a,\Lambda_c}\begin{pmatrix}G_{a,\Lambda_c}(r)\\ F_{a,\Lambda_c}(r)\end{pmatrix}\\ &= \begin{pmatrix}\Sigma_+^{\Lambda_c}(r) & -\frac{d}{dr}+\frac{\kappa_{a,\Lambda_c}}{r}\\ \frac{d}{dr}+\frac{\kappa_{a,\Lambda_c}}{r} & -\left[2M_{\Lambda_c}-\Sigma_-^{\Lambda_c}(r)\right]\end{pmatrix}\begin{pmatrix}G_{a,\Lambda_c}(r)\\ F_{a,\Lambda_c}(r)\end{pmatrix}.\end{aligned} \tag{12}$$

Here, the self-energies $\Sigma_\pm^{\Lambda_c} = \Sigma_{0,\Lambda_c} \pm \Sigma_{S,\Lambda_c}$ of the Λ_c^+ hyperon are composed by the vector and scalar terms. The scalar self-energy $\Sigma_{S,\Lambda_c} = \Sigma^\sigma_{S,\Lambda_c}$, and the time component of the vector one is given by

$$\Sigma_{0,\Lambda_c}(r) = \sum_\varphi \Sigma^\varphi_{0,\Lambda_c}(r) + \Sigma_R(r), \tag{13}$$

where $\varphi = \omega^\mu, A^\mu$ for the Λ_c^+ hyperon. Specifically, the contributions to the self-energy from isoscalar mesons (σ and ω^μ) as well as photon can be expressed as

$$\Sigma^\sigma_{S,\Lambda_c}(r) = -g_{\sigma\Lambda_c}(r)\sum_B\int r'^2dr' g_{\sigma B}(r')\rho_{s,B}(r')R^\sigma_{00}(r,r'), \tag{14a}$$

$$\Sigma^\omega_{0,\Lambda_c}(r) = +g_{\omega\Lambda_c}(r)\sum_B\int r'^2dr' g_{\omega B}(r')\rho_{b,B}(r')R^\omega_{00}(r,r'), \tag{14b}$$

$$\Sigma^A_{0,\Lambda_c}(r) = +e\sum_B\int r'^2dr' e\rho_{b,B}(r')Q_B R^A_{00}(r,r'). \tag{14c}$$

Here, $\rho_{s,B}$ and $\rho_{b,B}$ represent the scalar and baryon densities, respectively.

In the DDRMF framework, to ensure self-consistency between the energy density functional and single-particle properties, additional rearrangement terms are introduced into the baryon self-energies due to the density-dependent coupling strengths [105]. For the Λ_c^+ hypernucleus, the rearrangement term Σ_R includes contributions from both nucleon, Σ_R^N, and hyperon, $\Sigma_R^{\Lambda_c}$. For the nucleon, contributions from various coupling channels need to be considered, whereas for the hyperon the contribution arises solely from the isoscalar coupling channels. Here, for the sake of simplicity, only the contributions from the Λ_c^+ hyperon are provided,

$$\begin{aligned}\Sigma_R^{\Lambda_c}(r) &= \frac{1}{g_{\sigma\Lambda_c}}\frac{\partial g_{\sigma\Lambda_c}}{\partial\rho_b}\rho_{s,\Lambda_c}\Sigma^\sigma_{S,\Lambda_c}(r)\\ &\quad + \frac{1}{g_{\omega\Lambda_c}}\frac{\partial g_{\omega\Lambda_c}}{\partial\rho_b}\rho_{b,\Lambda_c}\Sigma^\omega_{0,\Lambda_c}(r).\end{aligned} \tag{15}$$

III. RESULTS AND DISCUSSION

In this section, we extend the DDRMF theory to include the degrees of freedom of the Λ_c^+ hyperon. By combining the results of microscopic first-principle calculations, we construct effective DDRMF $\Lambda_c N$ interactions. Based on this, we conduct a thorough discussion on the existence and stability of Λ_c^+ hypernuclei, as well as explore the description of bulk and single-particle properties for bound hypernuclei. To effectively account for the impact of nuclear in-medium effects on the description of hypernuclear structures, we select several sets of density-dependent Lagrangians for NN effective interactions, including TW99 [105], PKDD [106], DD-LZ1 [107], DD-ME2 [108], DD-MEX [109,110], and DD-MEδ [78]. Among these models, the effective interaction DD-MEδ includes a more comprehensive contribution of meson-nucleon coupling channels by introducing the isovector scalar δ meson. Specifically, the Dirac equation is solved in a radial box of size $R = 20$ fm with a step of 0.1 fm.

For the nonmagic-number hypernuclei discussed in this work, namely $^{52}_{\Lambda_c}$Cr, $^{90}_{\Lambda_c}$Zr, $^{91}_{\Lambda_c}$Nb, and $^{140}_{\Lambda_c}$Ce, the BCS method is applied for the nucleon's pairing correlations, by considering only nn and pp pairing with the Gogny interaction D1S [111,112]. To achieve more proper treatment of the hypernuclei with open-shell nuclear cores, it is important to consider not only the pairing correlations but also the deformation of the systems. Because most research on charmed hypernuclei is based on the spherical symmetry approximation, for the convenience of comparison with other works, this study also conducts analysis based on the spherical symmetry approximation. Furthermore, for hypernuclei with an odd number of protons, namely $^{52}_{\Lambda_c}$Cr, $^{90}_{\Lambda_c}$Zr, and $^{140}_{\Lambda_c}$Ce, the blocking effect should also be considered for the last valence proton. In detail, we check the binding energy by blocking various proton orbits near the Fermi surface, and select the one with the lowest binding as the ground state [28]. At the same time, it is assumed that the Λ_c^+ hyperon always occupies its ground state, specifically the $1s_{1/2}$ orbit, with a fixed occupancy probability of 1/2.

A. $\Lambda_c N$ effective interaction and stability of charmed hypernuclei

To achieve a theoretical description of hypernuclear structure, further development of the $\Lambda_c N$ interaction is required within the framework of RMF theory; this interaction can generally be expressed as the ratio of meson-hyperon and meson-nucleon coupling strengths. Since Λ_c^+ is an isospin-zero particle, only isoscalar mesons can participate in the $\Lambda_c N$ interaction within the meson-exchange diagram. Specifically, for the isoscalar vector ω^μ meson, the ratio of coupling strength is determined to be $R_{\omega\Lambda_c} = g_{\omega\Lambda_c}/g_{\omega N} = 0.666$ based on the naive quark model [51,52]. As for the isoscalar scalar σ meson, its coupling strength is generally determined from experimental data. However, the available experimental data for the Λ_c^+ hypernucleus are currently quite limited, and there is insufficient evidence to confirm the observation of bound Λ_c^+ hypernuclei. Thus, alternative approaches are needed to construct the $\Lambda_c N$ interaction. As mentioned in the Introduction, results obtained from lattice QCD simulations combined with chiral effective field theory extrapolation provide a possible reference [54,56]. To investigate the properties of the $\Lambda_c N$ interaction in nuclear matter, subsequent work has used the Brueckner-Hartree-Fock method to obtain the Λ_c^+ hyperon potential U_{Λ_c} in symmetric nuclear matter at finite density [54]. This serves as a bridge for studying Λ_c^+ hypernuclei using first-principles calculations and RMF theory. By fitting the empirical Λ_c^+ hyperon potential obtained from first-principles calculations at specific densities or Fermi momenta, the $\Lambda_c N$ interaction can be effectively constructed.

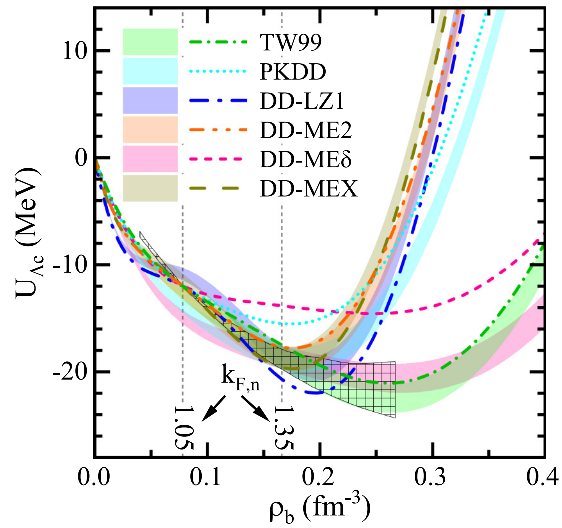

FIG. 1. The Λ_c^+ potentials U_{Λ_c} as a function of the baryon density ρ_b in symmetric nuclear matter, calculated by the $\Lambda_c N$ effective interactions within DDRMF models. The lines represent the results from $\Lambda_c 1$, while the shaded regions correspond to $\Lambda_c 2$. The square grid area indicates the empirical constraints of the Λ_c^+ potential extracted from Fig. 1(a) in Ref. [54].

Within the framework of DDRMF theory, the Λ_c^+ hyperon potential in symmetric nuclear matter can be expressed as

$$U_{\Lambda_c} = \sum_B \left[-g_{\sigma\Lambda_c}\frac{g_{\sigma B}}{m_\sigma^2}\rho_{s,B} + g_{\omega\Lambda_c}\frac{g_{\omega B}}{m_\omega^2}\rho_{b,B} + \frac{1}{\rho_0}\left(-\frac{g_{\sigma B}}{m_\sigma^2}\rho_{s,B}^2\frac{\partial g_{\sigma B}}{\partial \xi} + \frac{g_{\omega B}}{m_\omega^2}\rho_{b,B}^2\frac{\partial g_{\omega B}}{\partial \xi}\right)\right], \quad (16)$$

where the terms involving density derivatives arise from the contributions of the rearrangement terms. According to Eq. (16), the σ-Λ_c coupling strength can be determined by fitting the empirical hyperon potential in symmetric nuclear matter, as presented in Fig. 1(a) of Ref. [54]. It is worth noting that, due to the utilization of different cutoff values ($\Lambda = 500$ MeV or $\Lambda = 600$ MeV) in handling the hyperon-nucleon interaction, there exists some uncertainty in the evolution of the empirical hyperon potential with Fermi momentum. For clarity in discussion, the data from empirical hyperon potential have been extracted and showcased as a square grid in Fig. 1.

Notably, at Fermi momentum $k_{F,n} = 1.05$ fm^{-1}, the empirical hyperon potentials coincide for both cutoff values, while the differences between potentials become more pronounced as the Fermi momentum moves towards smaller or larger regions. To minimize additional influences when constructing the $\Lambda_c N$ interaction, we first fit the empirical hyperon potential at Fermi momentum $k_{F,n} = 1.05$ fm^{-1} with $U_{\Lambda_c} = -11.98$ MeV, yielding a series of effective $\Lambda_c N$ interactions labeled as $\Lambda_c 1$. For comparison, we also introduced another fitting target by selecting the empirical potential at Fermi momentum $k_{F,n} = 1.35$ fm^{-1}, as reported at the corresponding

TABLE I. The σ-Λ_c coupling strengths $R_{\sigma\Lambda_c}$ fitted for several DDRMF effective interactions according to the empirical constraints of the Λ_c^+ potential U_{Λ_c} in symmetric nuclear matter [54]. In detail, the series Λ_c1 is determined by the fixed potential $U_{\Lambda_c} = -11.98$ MeV at $k_{F,n} = 1.05$ fm^{-1}, while two values of Λ_c2 which define the lower and upper limits are given by fitting $U_{\Lambda_c} = -17.60$ or -19.70 MeV at $k_{F,n} = 1.35$ fm^{-1}, respectively. In addition, the Λ_c^+ Dirac effective masses $M^*_{\Lambda_c}/M_{\Lambda_c}$ and Λ_c^+ potentials U_{Λ_c} (in MeV) in symmetric nuclear matter at saturation density are summarized as well.

		Λ_c1	Λ_c2	
TW99	$R_{\sigma\Lambda_c}$	0.5847	0.5849	0.5897
	$M^*_{\Lambda_c}/M_{\Lambda_c}$	0.8936	0.8936	0.8927
	U_{Λ_c}	−16.69	−16.77	−18.78
PKDD	$R_{\sigma\Lambda_c}$	0.5836	0.5885	0.5934
	$M^*_{\Lambda_c}/M_{\Lambda_c}$	0.8977	0.8968	0.8960
	U_{Λ_c}	−15.21	−17.18	−19.16
DD-LZ1	$R_{\sigma\Lambda_c}$	0.5908	0.5836	0.5885
	$M^*_{\Lambda_c}/M_{\Lambda_c}$	0.8924	0.8937	0.8928
	U_{Λ_c}	−19.98	−17.00	−19.03
DD-ME2	$R_{\sigma\Lambda_c}$	0.5878	0.5876	0.5925
	$M^*_{\Lambda_c}/M_{\Lambda_c}$	0.8968	0.8968	0.8959
	U_{Λ_c}	−17.24	−17.16	−19.13
DD-MEX	$R_{\sigma\Lambda_c}$	0.5902	0.5857	0.5905
	$M^*_{\Lambda_c}/M_{\Lambda_c}$	0.8923	0.8931	0.8922
	U_{Λ_c}	−18.98	−17.10	−19.11
DD-MEδ	$R_{\sigma\Lambda_c}$	0.5799	0.5896	0.5951
	$M^*_{\Lambda_c}/M_{\Lambda_c}$	0.9069	0.9053	0.9044
	U_{Λ_c}	−13.65	−17.21	−19.23

nuclear saturation density in Ref. [54]. This selection yielded a set of effective $\Lambda_c N$ interactions, which are labeled as Λ_c2. The comparison between Λ_c1 and Λ_c2 could illustrate the impact of uncertain in-medium $\Lambda_c N$ interactions on the prediction of hypernuclear properties. Due to the errors in the empirical hyperon potential arising from different Λ cutoff values, Λ_c2 exhibits a certain level of uncertainty. Its upper and lower limits are obtained by fitting $U_{\Lambda_c} = -19.70$ MeV and $U_{\Lambda_c} = -17.60$ MeV of the empirical hyperon potential, respectively. One should notice that the value of $k_{F,n} = 1.35$ fm^{-1} in Ref. [54] does not exactly correspond to nuclear saturation density (but almost nearby) for the selected sets of RMF effective Lagrangians, and such distinction needs to be taken into account in subsequent discussions.

Based on the selection of several DDRMF effective interactions, the ratios of the σ-Λ_c coupling strength $R_{\sigma\Lambda_c}$ determined by the above-mentioned fitting strategies are shown in Table I. Additionally, the table summarizes the effective masses $M^*_{\Lambda_c}/M_{\Lambda_c}$ for hyperon obtained from various effective interactions, as well as the hyperon potential U_{Λ_c} at each model's saturation density. It is observed that, for both Λ_c1 and Λ_c2, the $R_{\sigma\Lambda_c}$ provided by various DDRMF effective interactions exhibit significant differences, which affect the description of nuclear matter properties such as the effective mass and hyperon potential. Due to the relatively large mass of the Λ_c^+ particle, the effective mass, despite showing some differences, does not exhibit a sensitive dependence on $R_{\sigma\Lambda_c}$. In contrast, the hyperon potential is significantly dependent on the strength of the $\Lambda_c N$ interaction, especially for the effective interaction Λ_c1. Although all the DDRMF Λ_c1 Lagrangians are fitted to the empirical hyperon potential at the minimum uncertainty, there are significant variations in the hyperon potential at saturation density as the baryon density evolves, ranging from −13.65 to −19.98 MeV for different effective interactions. To reduce theoretical uncertainties, it is necessary to identify some model-sensitive observables in the future to impose additional constraints.

To gain a more intuitive understanding of the differences in the effective $\Lambda_c N$ interactions among various DDRMF models, Fig. 1 shows the evolution of the Λ_c^+ hyperon potential as a function of baryon density ρ_b in symmetric nuclear matter. The lines represent the results for effective interaction Λ_c1, while the results for Λ_c2 are indicated by the shaded region. For Λ_c1, the interaction is obtained by fitting the empirical hyperon potential at a Fermi momentum of $k_{F,n} = 1.05$ fm^{-1}, resulting in a general consistency of the hyperon potential at low densities across various DDRMF models, except for DD-LZ1. However, as the hyperon potential evolves towards higher baryon densities, discrepancies among the models quickly emerge, with significant differences already evident in the subsaturation region. For Λ_c2, the interaction is derived by fitting the empirical hyperon potential at $k_{F,n} = 1.35$ fm^{-1}, and its results show significant model dependence at both high and low densities.

Since this work focuses on the existence of Λ_c^+ hypernuclei and their structural properties, we first examine the behavior of the $\Lambda_c N$ effective interaction in regions below saturation density. By analyzing the results of Λ_c1 and Λ_c2, we can understand the impact of the uncertainty in the hyperon potential at saturation and low densities on the description of hypernuclear structures. It is worth noting that both Λ_c1 and Λ_c2 show the most significant differences in the hyperon potential below saturation density for the DD-LZ1 and DD-MEδ models, which might reflect the uncertainty of the DDRMF theory in regions below saturation density. In contrast, TW99 and DD-ME2 exhibit the smallest differences in the hyperon potential below saturation density, and the results for Λ_c1 and Λ_c2 are largely consistent. In the subsequent discussion, we will select these four typical effective interactions for further analysis. When looking at the curves at higher densities above saturation, the evolution of U_{Λ_c} with baryon density obtained from various DDRMF functionals splits into two branches. The Λ_c^+ hyperon potential becomes repulsive at baryon densities exceeding 0.4 fm^{-3} for TW99 and DD-MEδ, whereas it turns repulsive at significantly lower densities for the other RMF effective Lagrangians.

The evolution of the Λ_c^+ hyperon potential in symmetric nuclear matter, as described by Eq. (16), can be qualitatively understood through the density dependence of the coupling strengths. Based on the Λ_c1 effective interaction, Fig. 2 illustrates the variation of meson-Λ_c coupling strengths with baryon density for different DDRMF models. In the subsaturation density region, the rearrangement term contributes primarily as a weak repulsion, and the depth of the hyperon potential is primarily determined by the magnitude of the coupling strength. Due to the relatively large Dirac effective

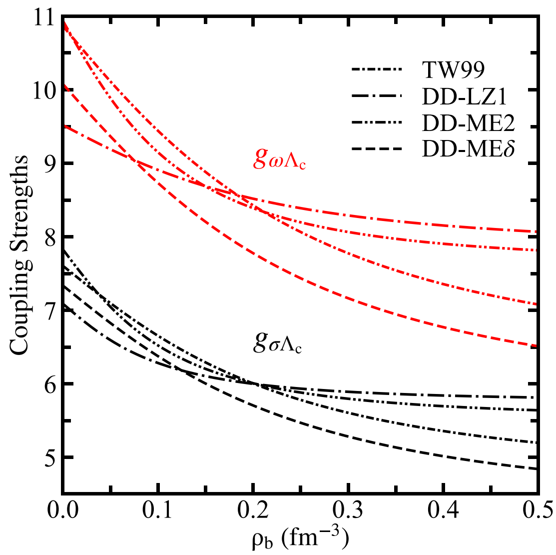

FIG. 2. The baryon density dependence of meson-Λ_c coupling strengths, namely, the isoscalar $g_{\sigma\Lambda_c}$ (black lines) and $g_{\omega\Lambda_c}$ (red lines), for the $\Lambda_c N$ effective interactions $\Lambda_c 1$ within DDRMF models.

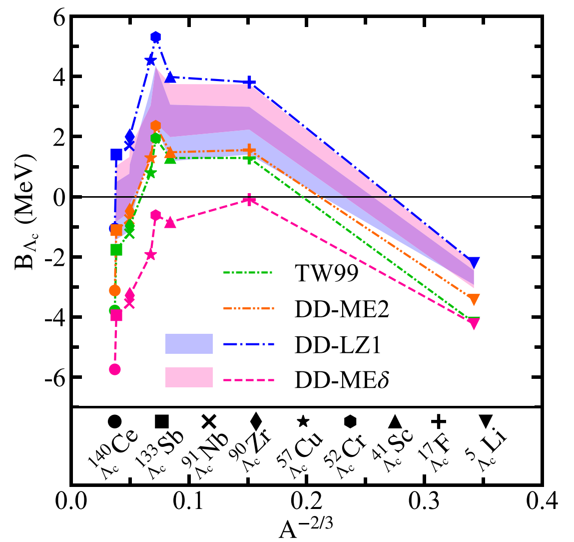

FIG. 3. The calculated Λ_c^+ separation energies B_{Λ_c} for the ground state of charmed hypernuclei with various DDRMF effective interactions. The lines represent the results of the $\Lambda_c 1$ model, whereas the shaded areas with just two examples (DD-LZ1 and DD-MEδ) correspond to those from $\Lambda_c 2$.

masses of baryons in this density region, the attractive σ potential is stronger. When this large σ attraction competes with and balances the repulsive ω potential, a weak attractive hyperon potential forms in the subsaturation density region. As the baryon density approaches saturated, the repulsive effect from the rearrangement term diminishes, and even transforms into a weak attraction, with the attractive contribution increasing as density rises.

When density goes above saturation, Fig. 2 indicates that the decrease of the meson-Λ_c coupling strengths with density becomes slow. Thus, the rearrangement term's contribution reaches saturation at large baryon density, and the first two terms in Eq. (16) dominate the trend. As baryon density rises, the Dirac effective mass of baryons decreases, leading to a saturation of the σ attractive contribution, while the ω repulsive contribution continues to strengthen. Finally, the hyperon potential U_{Λ_c} becomes repulsive at high densities. Taking TW99 and DD-ME2 as examples, we further analyzed the factors leading to the significant differences in the hyperon potentials given by different models at high densities. As shown in Fig. 2, the decreasing trend in $g_{\omega\Lambda_c}$ is significantly greater in TW99 than in DD-ME2, resulting in a stronger attraction in TW99 at large densities. In fact, the more pronounced density dependence of the meson-Λ_c coupling in TW99 also enhances the attractive contribution from the rearrangement term, making the hyperon potential more attractive overall in the high-density region. These results indicate that despite relevantly tight constraints on the hyperon potential at low and near saturation densities, different treatments of nuclear in-medium effects can lead to model discrepancies at high densities. To achieve more reliable theoretical description of nuclear matter and nuclear structure across various density ranges, it is essential to handle nuclear in-medium effects appropriately.

We now conduct an further discussion on the existence of bound Λ_c^+ hypernuclei using the four typical DDRMF Lagrangians, namely TW99, DD-ME2, DD-LZ1, and DD-MEδ, combined with the $\Lambda_c N$ effective interaction. Generally, the existence of bound hypernuclei can be determined by the separation energy B_{Λ_c} of the Λ_c^+ hyperon. The separation energy B_{Λ_c} is defined as the difference in binding energies, which is expressed as follows:

$$B_{\Lambda_c}\left[{}^{A}_{\Lambda_c}Z\right] \equiv E[{}^{A-1}(Z-1)] - E\left[{}^{A}_{\Lambda_c}Z\right]. \qquad (17)$$

Here, the nucleonic core is represented as ${}^{A-1}(Z-1)$, and the corresponding hypernucleus is denoted as ${}^{A}_{\Lambda_c}Z$. Based on the aforementioned four sets of DDRMF Lagrangians and the $\Lambda_c N$ effective interactions listed in Table I, the hyperon separation energies for charmed hypernuclei with different mass numbers are presented in Fig. 3. Among the various DDRMF functionals, the most significant differences in the hyperon potentials are observed between DD-LZ1 and DD-MEδ, which greatly influence the description of the Λ_c^+ hypernuclear bulk and single-particle properties, and these differences can be considered as sources of uncertainty in the DDRMF theory. Therefore, only the results based on DD-LZ1 and DD-MEδ are shown for $\Lambda_c 2$.

From Fig. 3, it is evident that the results for $\Lambda_c 1$, corresponding to different DDRMF Lagrangians, exhibit stronger model dependence compared to $\Lambda_c 2$. This is because $\Lambda_c 1$ is obtained by fitting the empirical hyperon potential at $k_{F,n} = 1.05\ \text{fm}^{-1}$, corresponding to a relatively low baryon density. As the baryon density evolves towards the region of saturation density, various DDRMF functionals quickly diverge in their predictions for the hyperon potential. In fact, the hyperons in bound Λ_c^+ hypernuclei are mainly distributed within the nucleus, where the nuclear medium density is close to saturation density. Consequently, the description of hyperon separation

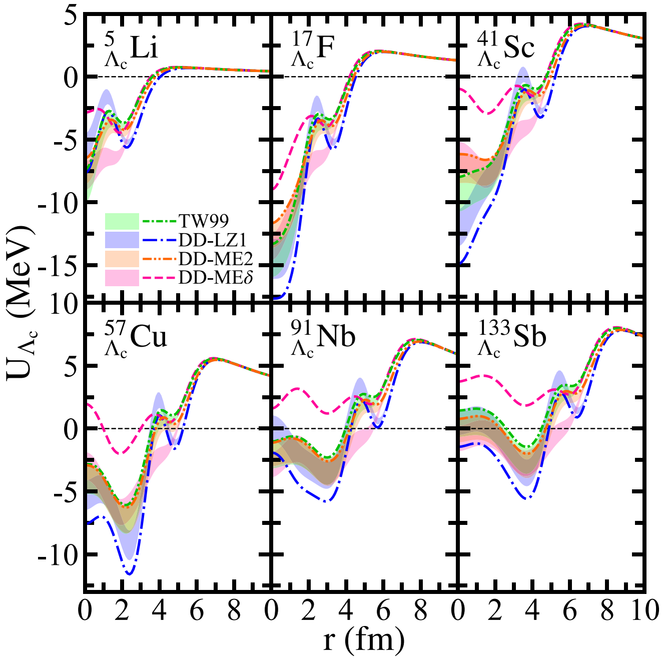

FIG. 4. The Λ_c^+ mean-field potentials in charmed hypernuclei $^{5}_{\Lambda_c}$Li, $^{17}_{\Lambda_c}$F, $^{41}_{\Lambda_c}$Sc, $^{57}_{\Lambda_c}$Cu, $^{91}_{\Lambda_c}$Nb, $^{133}_{\Lambda_c}$Sb as a function of radial coordinate r with various DDRMF effective interactions. The lines represent the results of the Λ_c1 model, whereas the shaded areas correspond to those from Λ_c2.

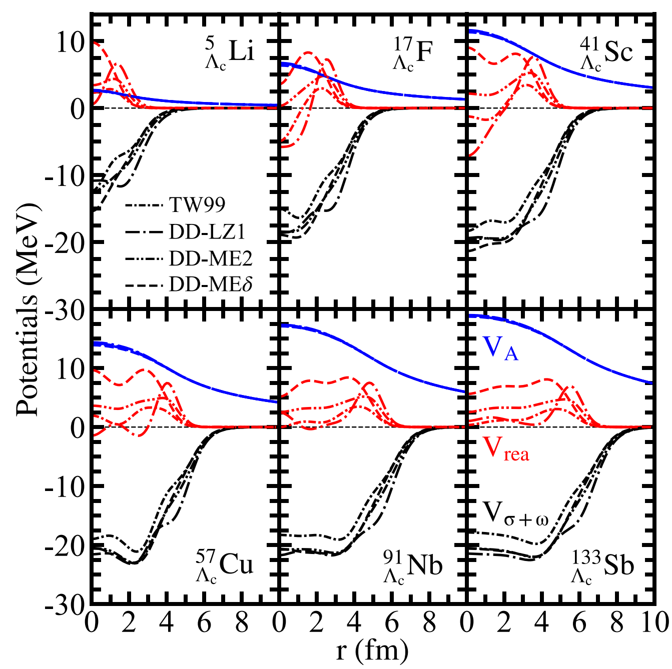

FIG. 5. The decomposition of the Λ_c^+ mean-field potentials for charmed hypernuclei $^{5}_{\Lambda_c}$Li, $^{17}_{\Lambda_c}$F, $^{41}_{\Lambda_c}$Sc, $^{57}_{\Lambda_c}$Cu, $^{91}_{\Lambda_c}$Nb, $^{133}_{\Lambda_c}$Sb, using four selected DDRMF effective interactions. The contributions from σ and ω mesons are denoted as $V_{\sigma+\omega}$ (black curves), the Coulomb potentials as $V_{\rm A}$ (blue), and those from the rearrangement terms as $V_{\rm rea}$ (red) due to the density dependence of meson-Λ_c couplings.

energies is closely related to the effective Λ_cN interaction at saturation density. Comparing the results of several DDRMF Lagrangians, it can be seen that, for hyperon separation energies, TW99 and DD-ME2 yield very similar results. This consistency is due to the similar behavior of their hyperon potentials under symmetric nuclear matter. However, DD-LZ1 and DD-MEδ show significant differences in their results. Compared to Λ_c1, the effective interaction Λ_c2 obtained by fitting the empirical hyperon potential near saturation density significantly reduces uncertainty, indicating that it may introduce less model dependence in the description of hypernuclear structures. Furthermore, the maximum Λ_c^+ hyperon separation energy obtained from the DDRMF functionals is approximately 5 MeV, which closely aligns with the conclusion of $0.6U_\Lambda$ in Ref. [50].

B. Properties of the charmed hypernuclei

To further understand the bulk and single-particle properties of hypernuclei, based on four typical DDRMF models, namely TW99, DD-ME2, DD-LZ1, and DD-MEδ, the hyperon potentials for several representative Λ_c^+ hypernuclei are presented, as shown in Fig. 4. It can be seen that, as the mass number increases, the depth of the hyperon potentials initially increases and then decreases, eventually becoming unbound. Comparing the various DDRMF models, it is found that the DD-MEδ-Λ_c1 model provides a relatively shallow hyperon potential, whereas DD-LZ1-Λ_c1 exhibits the opposite trend. As a result, DD-MEδ-Λ_c1 predicts unbound results for the studied Λ_c^+ hypernuclei, while DD-LZ1-Λ_c1 suggests the existence of Λ_c^+ hypernuclei across a wider range of masses. Furthermore, it is observed across all DDRMF models that the hyperon potentials generally exhibit peaks near the surface. These peaks extend to larger radial distances with increasing hypernuclear mass number, and at these larger radial distances the hyperon potentials consistently contribute repulsively. Further analysis of this phenomenon will be conducted in subsequent discussions.

To clarify the factors affecting hypernuclear stability, the contributions to the hyperon potential can be further decomposed. Since Λ_c^+ is a positively charged particle with zero isospin, the hyperon potential includes contributions from isoscalar mesons (σ and ω^μ) and photon (A^μ). Besides, the rearrangement term arising from the density dependence of the meson-baryon coupling strengths also needs to be considered. Based on four typical DDRMF models, and using Λ_c1 as an example, a series of hypernuclei ranging from $^{5}_{\Lambda_c}$Li to $^{133}_{\Lambda_c}$Sb were selected. The hyperon potential was decomposed into contributions from isoscalar mesons ($V_{\sigma+\omega}$), Coulomb interaction ($V_{\rm A}$), and rearrangement terms ($V_{\rm rea}$), as shown in Fig. 5. It can be observed that as the mass number of the hypernuclei increases, $V_{\sigma+\omega}$ gradually deepens and saturates at around -20 MeV. The contribution from Coulomb repulsion $V_{\rm A}$ also gradually increases, becoming a significant factor affecting the stability of heavy hypernuclei. As for the rearrangement terms $V_{\rm rea}$, they mainly provide repulsive contributions, peaking at about 10 MeV near the hypernuclear surface. This phenomenon accounts for the presence of peaks in the hyperon potential near the nuclear surface.

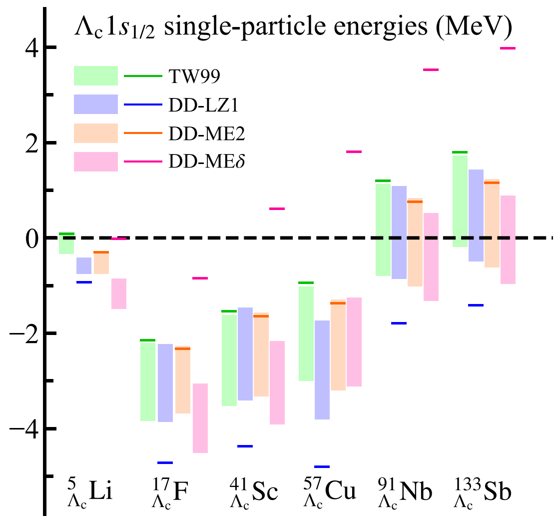

FIG. 6. The Λ_c^+ single-particle energies of $1s_{1/2}$ state in charmed hypernuclei $^{5}_{\Lambda_c}$Li, $^{17}_{\Lambda_c}$F, $^{41}_{\Lambda_c}$Sc, $^{57}_{\Lambda_c}$Cu, $^{91}_{\Lambda_c}$Nb, $^{133}_{\Lambda_c}$Sb are presented with the selected DDRMF effective interactions. The horizontal lines depict the results of Λ_c1, and the histogram areas represent ones from Λ_c2.

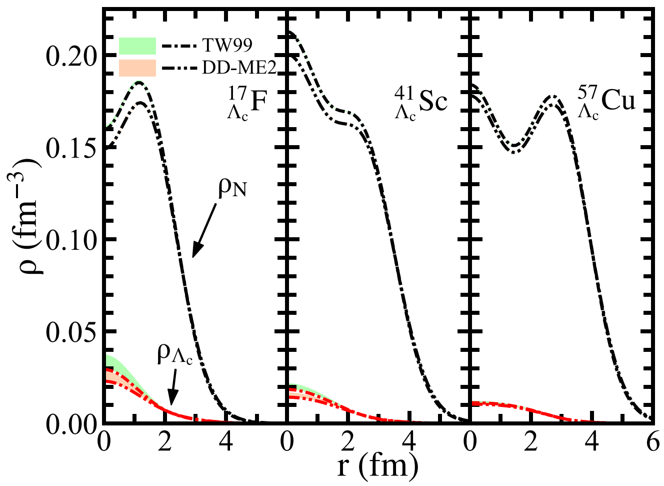

FIG. 7. The nucleon (neutron and proton) and hyperon (Λ_c^+) densities in charmed hypernuclei $^{17}_{\Lambda_c}$F, $^{41}_{\Lambda_c}$Sc, $^{57}_{\Lambda_c}$Cu obtained by the DDRMF effective interactions TW99 and DD-ME2. The solid lines are derived from the Λ_c1 model, while the shaded areas represent results from Λ_c2.

Comparing the contributions in light hypernuclei, it is found that the repulsive contribution from the rearrangement term is comparable to, or even exceeds, the Coulomb interaction. This indicates the crucial role of the rearrangement term in describing the stability of light hypernuclei. In fact, the contribution of the rearrangement term can be qualitatively explained by the density-dependent behavior of the coupling strengths shown in Fig. 2 and Eq. (15). At the nuclear surface, the drastic evolution of the coupling strength in low-density situations significantly alters the contribution of the rearrangement term.

In conjunction with the hyperon potentials, the corresponding Λ_c^+ single-particle energies for the $1s_{1/2}$ state are depicted in Fig. 6. It is observed that the single-particle energies initially decrease and then increase, aligning with the trend of the hyperon potentials shown in Fig. 4. Furthermore, for Λ_c1, the energy levels given by different models show significant variations compared to those for Λ_c2. These results also indicate that the uncertainty in hyperon potentials within nuclear matter at $k_{F,n} = 1.35$ fm^{-1}, as illustrated in Fig. 1, significantly influences the single-particle properties of the Λ_c^+ hyperon. In addition to the Λ_cN interaction, differences in NN interactions may also significantly affect the stability of the Λ_c^+ hypernucleus. When the Λ_cN interaction is specified, that is, when fitting the same U_{Λ_c}, we observe that the NN interactions from these models exhibit varying density-dependent behaviors. Variations in the NN interactions could potentially alter the distribution of the Λ_c^+ potential, which in turn could affect the single-particle properties of the hyperon. Subsequently, taking $^{57}_{\Lambda_c}$Cu as an example, we selected the DD-LZ1-Λ_c1 and DD-MEδ-Λ_c1 models, which show the most significant differences, to further elucidate the factors affecting the description of hyperon single-particle energy levels. From the hyperon potential decomposition, as shown in Fig. 5, it is found that these two models give comparable results for both $V_{\sigma+\omega}$ and $V_{\rm A}$, while there is a significant difference in $V_{\rm rea}$.

We can also compare the DDRMF results with other reference calculations. We chose the effective interactions that are more consistent with the range of Λ_c^+ potentials reported by Ref. [54], specifically TW99 and DD-ME2. Although the evolved trend of single-particle energy levels with mass number is similar, DDRMF models indicate weaker Λ_c^+ binding than the literature [54]. The heaviest predicted bound hypernucleus is $^{133}_{\Lambda_c}$Sb for DDRMF, whereas in Ref. [54] the heaviest bound one could reach approximately $^{209}_{\Lambda_c}$Bi. The results indicate that the treatment of medium effects related to the Λ_c^+ hyperon at finite densities can significantly influence predictions regarding the existence of hypernuclei.

In addition to affecting the single-particle energy levels of the Λ_c^+ hyperon, the nuclear many-body model and the uncertainties in Λ_cN interactions also result in variations in the description of the bulk properties of hypernuclei. To illustrate this, the DDRMF models TW99 and DD-ME2, along with the effective Λ_cN interaction, were used to determine the density distributions of the hyperon and nucleons in $^{17}_{\Lambda c}$F, $^{41}_{\Lambda c}$Sc, and $^{57}_{\Lambda c}$Cu, as shown in Fig. 7. As the mass number of the hypernucleus increases, the nucleon density gradually extends outward. The strong interaction between nucleons and hyperon causes the hyperon density distribution to become more diffuse, resulting in a corresponding decrease in the central hyperon density. Furthermore, it can be observed that the central hyperon density predicted by DD-ME2 is consistently lower than that predicted by TW99. This implies that the hyperon within the nucleus is more dispersed according to the predictions of DD-ME2, and a similar conclusion can be inferred from the nucleon density distributions. Additionally, for Λ_c2, the uncertainty in hyperon densities also decreases when increasing the mass number. This reduction in uncertainty is mainly because Λ_c^+ densities extend to larger radii, where the significance of the large potential difference

TABLE II. The binding energies E, single-particle energies $\varepsilon_{\text{s.p.}}$ of the $\Lambda_c^+ 1s_{1/2}$ state, matter radii R_m, hyperon radii R_{Λ_c}, and charge radii R_c for the charmed hypernuclei with two DDRMF models TW99 and DD-ME2, accompanied by the results for their core of normal nuclei. The $\Lambda_c N$ effective interactions $\Lambda_c 1$ are used. The radii are provided in units of fm, and energies are in MeV.

	TW99					DD-ME2				
	E	$\varepsilon_{\text{s.p.}}$	R_m	R_{Λ_c}	R_c	E	$\varepsilon_{\text{s.p.}}$	R_m	R_{Λ_c}	R_c
$^{17}_{\Lambda_c}$F	−124.576	−2.151	2.544	2.569	2.679	−129.302	−2.327	2.599	2.686	2.728
^{16}O	−123.286		2.553		2.687	−127.750		2.594		2.727
$^{41}_{\Lambda_c}$Sc	−335.282	−1.543	3.283	2.719	3.417	−344.087	−1.642	3.336	2.873	3.467
^{40}Ca	−333.993		3.302		3.421	−342.608		3.346		3.464
$^{52}_{\Lambda_c}$Cr	−437.741	−2.104	3.486	2.762	3.547	−444.951	−2.448	3.529	2.837	3.589
^{51}V	−435.795		3.505		3.551	−442.589		3.543		3.588
$^{57}_{\Lambda_c}$Cu	−475.690	−0.943	3.562	2.821	3.688	−481.975	−1.375	3.601	2.873	3.727
^{56}Ni	−474.894		3.580		3.692	−480.682		3.614		3.727

at saturation density, as shown in Fig. 1, becomes less critical for heavier hypernuclei. As an extension, the binding energies of hypernuclei, single-particle energies of the $\Lambda_c^+ 1s_{1/2}$ state, and their corresponding characteristic radii are provided based on TW99-$\Lambda_c 1$ and DD-ME2-$\Lambda_c 1$, as presented in Table II. Considering the impurity effect induced by the Λ_c^+ hyperon, results for nucleonic cores are also provided. Compared to their nucleonic cores, the introduction of Λ_c^+ tends to reduce the matter radius of the hypernucleus. It is evident that the characteristic radii predicted by DD-ME2-$\Lambda_c 1$ are generally larger than those predicted by TW99-$\Lambda_c 1$. This observation aligns with the conclusions drawn from the hyperon and nucleon density distributions shown in Fig. 7. As the mass number increases, both sets of models indicate an increase in the matter radii of hypernuclei, while the radii of the Λ_c^+ hyperon show significant differences. For TW99-$\Lambda_c 1$ the hyperon radii increase gradually with the mass number, whereas for DD-ME2-$\Lambda_c 1$ the hyperon radii increase initially and then remain almost constant. One possible explanation for this discrepancy is the differing balance between Coulomb repulsion and strong attractive interactions in the two models.

IV. SUMMARY

In summary, we extend the DDRMF theory to include the degrees of freedom of the Λ_c^+ hyperon. The $\Lambda_c N$ effective interaction is obtained by fitting the empirical hyperon potential of Λ_c^+ in symmetric nuclear matter, based on first-principles calculations [54]. Due to the utilization of different cutoffs, the empirical hyperon potential of Λ_c^+ is not uniquely determined and carries certain uncertainties. To mitigate the uncertainties arising from the fitting process in constructing the $\Lambda_c N$ interaction, we have chosen the empirical hyperon potential with the minimum uncertainty as one of the fitting targets. Specifically, we selected the value at the Fermi momentum $k_{F,n} = 1.05\ \text{fm}^{-1}$ and denoted the resulting interaction as $\Lambda_c 1$. Considering the discussion of the bulk and single-particle properties of Λ_c^+ hypernuclei, we also selected the empirical hyperon potential at $k_{F,n} = 1.35\ \text{fm}^{-1}$ as another fitting target, and the obtained interaction is named $\Lambda_c 2$. Furthermore, we present the Λ_c^+ hyperon potential in symmetric nuclear matter, calculated by the DDRMF Lagrangian and the $\Lambda_c N$ effective interaction chosen in this work. We observed that the hyperon potentials derived from the DDRMF functionals DD-LZ1 and DD-MEδ often exhibit significant differences, which reflect the uncertainties introduced by the DDRMF theory when describing the structures of Λ_c^+ hypernuclei. In contrast, the hyperon potentials provided by TW99 and DD-ME2 show the smallest differences in the region below saturation density. Regarding $\Lambda_c 1$ and $\Lambda_c 2$, the hyperon potentials obtained from the two sets of interactions display significant model dependence near saturation density and in the lower density region, respectively. Exploring these aspects can help us comprehend the impact of interaction uncertainties in the hyperon potential at saturation and low densities on the description of hypernuclear structures.

Based on four typical DDRMF functionals, namely TW99, DD-ME2, DD-LZ1, and DD-MEδ, combined with the $\Lambda_c N$ effective interaction, we explore the existence and stability of bound Λ_c^+ hypernuclei. Since the medium density is complicated when the hyperon is located in its single-particle orbit, the Λ_c^+ single-particle properties are quite sensitive to the detailed density-dependent behavior of the effective interactions. For $\Lambda_c 1$, significant differences in the hyperon potential provided by various DDRMF functionals below and around the saturation density affect the prediction for the existence of bound hypernuclei. For the interaction $\Lambda_c 2$, which is fitted to empirical hyperon potentials nearby the saturation density, the uncertainty among the results of various DDRMF functionals is significantly reduced. To further clarify the effects influencing the existence and stability of Λ_c^+ hypernuclei, we decompose the contributions of various components of the hyperon potential. Since the Λ_c^+ particle is positively charged and has isospin- zero, the hyperon potential can be decomposed into contributions from isoscalar mesons (σ and ω^μ), photons, and rearrangement terms introduced by the density dependence of the meson-baryon coupling strengths. For the studied Λ_c^+ hypernuclei, except for the light hypernucleus $^5_{\Lambda_c}$Li, the contribution from isoscalar mesons quickly saturates. Thus, the existence of hypernuclei depends on the contributions from Coulomb repulsion and the rearrangement terms. In light hypernuclei, the impact of the rearrangement terms is most significant. As the mass number increases, the contribution from Coulomb repulsion gradually becomes more dominant.

Furthermore, the bulk properties of Λ_c^+ hypernuclei are presented using TW99-Λ_c1 and DD-ME2-Λ_c1 effective interactions. It is found that the hyperon radius is more compact than the charge radius, and there is a reduction in the matter radius when compared to nucleonic cores. Moreover, the effect of introducing the Λ_c^+ hyperon on the nuclear charge radius exhibits variations between the two sets of effective interactions. Because the charmed baryon carries an additional unit positive charge, it creates a competition between attraction from meson-nucleon interactions and repulsion from Coulomb interactions, affecting the charge distribution of nucleonic cores differently. Ultimately, the Λ_c^+ radius tends to expand as the mass number increases, which is primarily driven by the escalating influence of Coulomb repulsion. In this work, the deformation effects of hypernuclei with open-shell nucleonic cores remain unexplored, which will be the subject of future investigations. For the interaction between charmed baryon and nucleon, the coupling channel $\Lambda_c N$-$\Sigma_c N$-$\Sigma_c^* N$ in addition to the $\Lambda_c N$ interactions has also been investigated in recent studies, which shows that the coupling channel is essential in $\Lambda_c N$ bound states [57]. Consequently, comprehensive research on charmed hypernuclei systems is necessary, considering the mixing effects between nucleons and different charmed baryons. Correspondingly, given the current uncertainty in $\Lambda_c N$ interaction research, it is hoped that more extensive theoretical and experimental research will be conducted in the future to refine the understanding of the $\Lambda_c N$ interaction.

ACKNOWLEDGMENTS

This work was partly supported by the Fundamental Research Funds for the Central Universities, Lanzhou University (lzujbky-2022-sp02, lzujbky-2023-stlt01), the National Natural Science Foundation of China (11875152), and the Strategic Priority Research Program of Chinese Academy of Sciences (XDB34000000).

[1] M. Danysz and J. Pniewski, Lond. Edinb. Dublin Philos. Mag. **44**, 348 (1953).
[2] Y. Yamamoto, T. Motoba, H. Himeno, K. Ikeda, and S. Nagata, Prog. Theor. Phys. Suppl. **117**, 361 (1994).
[3] B. Gibson and E. Hungerford, Phys. Rep. **257**, 349 (1995).
[4] M. Prakash, I. Bombaci, M. Prakash, P. J. Ellis, J. M. Lattimer, and R. Knorren, Phys. Rep. **280**, 1 (1997).
[5] J. M. Lattimer and M. Prakash, Science **304**, 536 (2004).
[6] L. Tolos and L. Fabbietti, Prog. Part. Nucl. Phys. **112**, 103770 (2020).
[7] R. Hayano, T. Ishikawa, M. Iwasaki, H. Outa, E. Takada, H. Tamura, A. Sakaguchi, M. Aoki, and T. Yamazaki, Phys. Lett. B **231**, 355 (1989).
[8] S. Aoki, S. Bahk, K. Chung, S. Chung, H. Funahashi, C. Hahn, T. Hara, S. Hirata, K. Hoshino, M. Ieiri *et al.*, Prog. Theor. Phys. **89**, 493 (1993).
[9] H. Takahashi, J. K. Ahn, H. Akikawa, S. Aoki, K. Arai, S. Y. Bahk, K. M. Baik, B. Bassalleck, J. H. Chung, M. S. Chung *et al.*, Phys. Rev. Lett. **87**, 212502 (2001).
[10] M. Yamaguchi, K. Tominaga, Y. Yamamoto, and T. Ueda, Prog. Theor. Phys. **105**, 627 (2001).
[11] O. Hashimoto and H. Tamura, Prog. Part. Nucl. Phys. **57**, 564 (2006).
[12] K. Nakazawa, Nucl. Phys. A **835**, 207 (2010).
[13] A. Feliciello and T. Nagae, Rep. Prog. Phys. **78**, 096301 (2015).
[14] A. Gal, E. V. Hungerford, and D. J. Millener, Rev. Mod. Phys. **88**, 035004 (2016).
[15] A. Gal and D. Millener, Phys. Lett. B **701**, 342 (2011).
[16] D. Millener, Nucl. Phys. A **881**, 298 (2012).
[17] R. Wirth, D. Gazda, P. Navrátil, A. Calci, J. Langhammer, and R. Roth, Phys. Rev. Lett. **113**, 192502 (2014).
[18] J. Cugnon, A. Lejeune, and H. J. Schulze, Phys. Rev. C **62**, 064308 (2000).
[19] H. J. Schulze and E. Hiyama, Phys. Rev. C **90**, 047301 (2014).
[20] T. T. Sun, E. Hiyama, H. Sagawa, H. J. Schulze, and J. Meng, Phys. Rev. C **94**, 064319 (2016).
[21] J. Schaffner, C. B. Dover, A. Gal, C. Greiner, and H. Stöcker, Phys. Rev. Lett. **71**, 1328 (1993).
[22] N. K. Glendenning, D. Von-Eiff, M. Haft, H. Lenske, and M. K. Weigel, Phys. Rev. C **48**, 889 (1993).
[23] J. Schaffner, C. Dover, A. Gal, C. Greiner, D. Millener, and H. Stocker, Ann. Phys. (NY) **235**, 35 (1994).
[24] E. N. E. van Dalen, G. Colucci, and A. Sedrakian, Phys. Lett. B **734**, 383 (2014).
[25] M. Fortin, S. S. Avancini, C. Providência, and I. Vidaña, Phys. Rev. C **95**, 065803 (2017).
[26] S. Y. Ding, W. Yang, and B. Y. Sun, Chin. Phys. C **47**, 124103 (2023).
[27] H. Shen and H. Toki, Nucl. Phys. A **707**, 469 (2002).
[28] S. Y. Ding, Z. Qian, B. Y. Sun, and W. H. Long, Phys. Rev. C **106**, 054311 (2022).
[29] E. G. Cazzoli, A. M. Cnops, P. L. Connolly, R. I. Louttit, M. J. Murtagh, R. B. Palmer, N. P. Samios, T. T. Tso, and H. H. Williams, Phys. Rev. Lett. **34**, 1125 (1975).
[30] B. Knapp, W. Lee, S. D. Smith, A. Wijangco, J. Knauer, D. Yount, J. Bronstein, R. Coleman, G. Gladding, M. Goodman *et al.*, Phys. Rev. Lett. **37**, 882 (1976).
[31] A. Hosaka, T. Hyodo, K. Sudoh, Y. Yamaguchi, and S. Yasui, Prog. Part. Nucl. Phys. **96**, 88 (2017).
[32] G. Krein, AIP Conf. Proc. **2130**, 020022 (2019).
[33] T. Bressani and F. Iazzi, Nuovo Cimento A **102**, 597 (1989).
[34] S. A. Bunyatov, V. V. Lyukov, N. I. Starkov, and V. A. Tsarev, Nuovo Cimento A **104**, 1361 (1991).
[35] Yu. A. Batusov, S. A. Bunyatov, V. V. Lyukov, V. M. Sidorov, A. A. Tyapkin, and V. A. Yarba, JETP Lett. **33**, 56 (1981).
[36] V. Lyukov, Nuovo Cimento A **102**, 583 (1989).
[37] U. Wiedner, Prog. Part. Nucl. Phys. **66**, 477 (2011).
[38] R. Shyam and K. Tsushima, Phys. Lett. B **770**, 236 (2017).
[39] J. Riedl, A. Schaefer, and M. Stratmann, Eur. Phys. J. C **52**, 987 (2007).
[40] H. Fujioka, K. Hicks, Y. Igarashi, K. Itahashi, T. K. Komatsubara, K. Miwa, T. Nagae, S. N. Nakamura, H. Nanjo, H. Noumi *et al.*, arXiv:1706.07916.

[41] C. B. Dover and S. H. Kahana, Phys. Rev. Lett. **39**, 1506 (1977).
[42] G. Bhamathi, Phys. Rev. C **24**, 1816 (1981).
[43] H. Bando and M. Bando, Phys. Lett. B **109**, 164 (1982).
[44] B. F. Gibson, C. B. Dover, G. Bhamathi, and D. R. Lehman, Phys. Rev. C **27**, 2085 (1983).
[45] H. Garcilazo, A. Valcarce, and T. F. Caramés, Phys. Rev. C **92**, 024006 (2015).
[46] S. Wu, Q. Wu, H. Huang, X. Chen, J. Ping, and Q. Wang, Phys. Rev. C **109**, 014001 (2024).
[47] K. Tsushima and F. C. Khanna, Phys. Rev. C **67**, 015211 (2003).
[48] L. Wu, J. Hu, and H. Shen, Phys. Rev. C **101**, 024303 (2020).
[49] H. Güven, K. Bozkurt, E. Khan, and J. Margueron, Phys. Rev. C **104**, 064306 (2021).
[50] Y. X. Liu, C. F. Chen, Q. B. Chen, H. T. Xue, H. J. Schulze, and X. R. Zhou, Phys. Rev. C **108**, 064312 (2023).
[51] Y. H. Tan, X. H. Zhong, C. H. Cai, and P. Z. Ning, Phys. Rev. C **70**, 054306 (2004).
[52] Y. H. Tan and P. Z. Ning, Europhys. Lett. **67**, 355 (2004).
[53] I. Vidaña, A. Ramos, and C. E. Jiménez-Tejero, Phys. Rev. C **99**, 045208 (2019).
[54] J. Haidenbauer, A. Nogga, and I. Vidana, Eur. Phys. J. A **56**, 195 (2020).
[55] N. Starkov and V. Tsarev, Nucl. Phys. A **450**, 507 (1986).
[56] J. Haidenbauer and G. Krein, Eur. Phys. J. A **54**, 199 (2018).
[57] Y. R. Liu and M. Oka, Phys. Rev. D **85**, 014015 (2012).
[58] S. Maeda, M. Oka, and Y. R. Liu, Phys. Rev. C **98**, 035203 (2018).
[59] R. Gatto and F. Paccanoni, Nuovo Cimento A **46**, 313 (1978).
[60] H. Bando, Prog. Theor. Phys. Suppl. **81**, 197 (1985).
[61] T. Miyamoto, S. Aoki, T. Doi, S. Gongyo, T. Hatsuda, Y. Ikeda, T. Inoue, T. Iritani, N. Ishii, D. Kawai *et al.*, Nucl. Phys. A **971**, 113 (2018).
[62] S. Yasui, Phys. Rev. C **100**, 065201 (2019).
[63] K. Ohtani, K. J. Araki, and M. Oka, Phys. Rev. C **96**, 055208 (2017).
[64] R. Brockmann and W. Weise, Phys. Lett. B **69**, 167 (1977).
[65] A. Bouyssy, Phys. Lett. B **99**, 305 (1981).
[66] N. K. Glendenning and S. A. Moszkowski, Phys. Rev. Lett. **67**, 2414 (1991).
[67] J. Mareš and B. K. Jennings, Phys. Rev. C **49**, 2472 (1994).
[68] Y. Sugahara and H. Toki, Prog. Theor. Phys. **92**, 803 (1994).
[69] D. Vretenar, W. Pöschl, G. A. Lalazissis, and P. Ring, Phys. Rev. C **57**, R1060 (1998).
[70] J. Hu, E. Hiyama, and H. Toki, Phys. Rev. C **90**, 014309 (2014).
[71] X. Y. Wu, H. Mei, J. M. Yao, and X. R. Zhou, Phys. Rev. C **95**, 034309 (2017).
[72] Z. X. Liu, C. J. Xia, W. L. Lu, Y. X. Li, J. N. Hu, and T. T. Sun, Phys. Rev. C **98**, 024316 (2018).
[73] R. Brockmann and H. Toki, Phys. Rev. Lett. **68**, 3408 (1992).
[74] W. H. Long, N. Van Giai, and J. Meng, Phys. Lett. B **640**, 150 (2006).
[75] L. W. Chen, C. M. Ko, and B. A. Li, Phys. Rev. C **76**, 054316 (2007).
[76] T. Nikšić, D. Vretenar, G. A. Lalazissis, and P. Ring, Phys. Rev. C **77**, 034302 (2008).
[77] B. Y. Sun, W. H. Long, J. Meng, and U. Lombardo, Phys. Rev. C **78**, 065805 (2008).
[78] X. Roca-Maza, X. Viñas, M. Centelles, P. Ring, and P. Schuck, Phys. Rev. C **84**, 054309 (2011).
[79] W. H. Long, B. Y. Sun, K. Hagino, and H. Sagawa, Phys. Rev. C **85**, 025806 (2012).
[80] Q. Zhao, B. Y. Sun, and W. H. Long, J. Phys. G: Nucl. Part. Phys. **42**, 095101 (2015).
[81] Z. W. Liu, Z. Qian, R. Y. Xing, J. R. Niu, and B. Y. Sun, Phys. Rev. C **97**, 025801 (2018).
[82] A. Li, J. N. Hu, X. L. Shang, and W. Zuo, Phys. Rev. C **93**, 015803 (2016).
[83] G. H. Zhang and W. Z. Jiang, Phys. Lett. B **720**, 148 (2013).
[84] S. Yang, B. N. Zhang, and B. Y. Sun, Phys. Rev. C **100**, 054314 (2019).
[85] S. Yang, X. D. Sun, J. Geng, B. Y. Sun, and W. H. Long, Phys. Rev. C **103**, 014304 (2021).
[86] G. Shen, C. J. Horowitz, and S. Teige, Phys. Rev. C **82**, 015806 (2010).
[87] M. Fortin, A. R. Raduta, S. Avancini, and C. Providência, Phys. Rev. D **101**, 034017 (2020).
[88] F. Hofmann, C. M. Keil, and H. Lenske, Phys. Rev. C **64**, 025804 (2001).
[89] S. S. Avancini, J. R. Marinelli, D. P. Menezes, M. M. W. Moraes, and C. Providência, Phys. Rev. C **75**, 055805 (2007).
[90] S. Wang, H. F. Zhang, and J. M. Dong, Phys. Rev. C **90**, 055801 (2014).
[91] W. Long, H. Sagawa, J. Meng, and N. V. Giai, Europhys. Lett. **82**, 12001 (2008).
[92] L. J. Wang, J. M. Dong, and W. H. Long, Phys. Rev. C **87**, 047301 (2013).
[93] J. J. Li, J. Margueron, W. H. Long, and N. Van Giai, Phys. Lett. B **753**, 97 (2016).
[94] S. S. Avancini, J. R. Marinelli, D. P. Menezes, M. M. W. Moraes, and A. S. Schneider, Phys. Rev. C **76**, 064318 (2007).
[95] F. Hofmann, C. M. Keil, and H. Lenske, Phys. Rev. C **64**, 034314 (2001).
[96] D. Vretenar, A. Afanasjev, G. Lalazissis, and P. Ring, Phys. Rep. **409**, 101 (2005).
[97] A. Afanasjev, S. Agbemava, D. Ray, and P. Ring, Phys. Lett. B **726**, 680 (2013).
[98] S. Yang, D. Wen, J. Wang, and J. Zhang, Phys. Rev. D **105**, 063023 (2022).
[99] C. J. Xia, B. Y. Sun, T. Maruyama, W. H. Long, and A. Li, Phys. Rev. C **105**, 045803 (2022).
[100] J. Cohen and H. J. Weber, Phys. Rev. C **44**, 1181 (1991).
[101] T. T. Sun, W. L. Lu, and S. S. Zhang, Phys. Rev. C **96**, 044312 (2017).
[102] K. Nakamura, K. Hagiwara, K. Hikasa, H. Murayama, M. Tanabashi, T. Watari, C. Amsler, M. Antonelli, D. M. Asner, H. Baer *et al.*, J. Phys. G: Nucl. Part. Phys. **37**, 075021 (2010).
[103] M. Abramowitz, *Handbook of Mathematical Functions with Formulas, Graphs, and Mathematical Tables* (National Bureau of Standards, Washington, 1964).
[104] D. A. Varshalovich, A. N. Moskalev, and V. K. Khersonskii, *Quantum Theory of Angular Momentum* (World Scientific, Singapore, 1988).
[105] S. Typel and H. Wolter, Nucl. Phys. A **656**, 331 (1999).
[106] W. Long, J. Meng, N. Van Giai, and S.-G. Zhou, Phys. Rev. C **69**, 034319 (2004).

[107] B. Wei, Q. Zhao, Z. H. Wang, J. Geng, B. Y. Sun, Y. F. Niu, and W. H. Long, Chin. Phys. C **44**, 074107 (2020).

[108] G. A. Lalazissis, T. Nikšić, D. Vretenar, and P. Ring, Phys. Rev. C **71**, 024312 (2005).

[109] A. Taninah, S. Agbemava, A. Afanasjev, and P. Ring, Phys. Lett. B **800**, 135065 (2020).

[110] I. A. Rather, U. Rahaman, M. Imran, H. C. Das, A. A. Usmani, and S. K. Patra, Phys. Rev. C **103**, 055814 (2021).

[111] J. Berger, M. Girod, and D. Gogny, Nucl. Phys. A **428**, 23 (1984).

[112] M. Bender, K. Rutz, P. Reinhard, and J. Maruhn, Eur. Phys. J. A **8**, 59 (2000).